UC Riverside

UC Riverside Electronic Theses and Dissertations

Title

CVD Growth of Graphene by Exfoliated Graphene Seeds on SiO2 Substrate

Permalink

https://escholarship.org/uc/item/9fc2j6c6

Author

Jahansouz, Setareh

Publication Date

2016

Peer reviewed|Thesis/dissertation

eScholarship.org Powered by the California Digital Library
University of California

UNIVERSITY OF CALIFORNIA
RIVERSIDE

CVD Growth of Graphene by Exfoliated Graphene Seeds on SiO_2 Substrate

A Thesis submitted in partial satisfaction
of the requirements for the degree of

Master of Science

in

Materials Science and Engineering

by

Setareh Jahansouz

March 2016

Thesis Committee:

Dr. Cengiz Ozkan, Chairperson
Dr. Mihri Ozkan
Dr. Kambiz Vafai
Dr. Krassimir N. Bozhilov

Copyright by
Setareh Jahansouz
2016

The Thesis of Setareh Jahansouz is approved:

Committee Chairperson

University of California, Riverside

Acknowledgements

Special thanks to Professor Cengiz Ozkan, Professor Mihri Ozkan, Dr. Isaac Ruiz, Zafer Mutlu, and those in the lab who helped me to complete my research and thesis processes.

ABSTRACT OF THE THESIS

CVD Growth of Graphene by Exfoliated Graphene Seeds on SiO2 Substrate

by

Setareh Jahansouz

Master of Science, Graduate Program in Materials Science and Engineering
University of California, Riverside, March 2016
Dr. Cengiz Ozkan, Chairperson

Graphene's unique mechanical, thermal and electrical properties make it an important material for research consideration. Additionally, the covalently bonded carbon atoms in graphene have potential applications in future technologies. Different methods have been proposed to synthesize graphene, but chemical vapor deposition (CVD) is the most promising. Chemical vapor deposition is recognized as low cost and is the most economical method. In this research, the growth of graphene on exfoliated graphene by a chemical vapor deposition method on SiO2 substrates has been shown as having a good potential to produce vertical stacking of graphene layers on top of exfoliated graphene seeds' flakes. This research will demonstrate experimental procedures, analytical techniques and supportive evidence to achieve vertical stacking of graphene-grown layers, on top of flakes after using chemical vapor deposition.

Contents

Figures

1-Introduction

Graphene is formed by a single layer of carbon atoms in two-dimensional honeycomb lattices [34]. 3-D materials like graphite composed of various layers of 2-D materials are produced in nature. Accordingly, two dimensional materials in most cases are not considered by researchers because of their instability characteristics. These materials are thermodynamically unstable and decompose under certain thickness limitations, and the single layers perform only as transient states fields [20, 27]. Hence, graphene is considered as a single layer of carbon atoms which are hexagonally bonded (see Figure 1), and graphite is included by stacking many graphene layers together [21,27]. It is extremely strong considering its low weight, it conducts electricity and heat with valuable efficiency, has remarkable mechanical features, and high conductivity field properties. Moreover, graphene is considered as a one atom layer thickness of graphite and as the fundamental structural of the other type of allotropes such as exfoliated graphene, carbon nanotubes, and graphite [5].

Fig1: Schematic of graphene

2-Graphene Synthesizes and Characterization

2-1-Graphene Motivations

Beginning in 2004, graphene changed from an "academic" material title to an important material in both applied and fundamental scientific studies. In 2004, free standing graphene produced by the technique of mechanical exfoliation was successfully introduced to those fields by Novoselov et al. [2]. Based on the Mermin-Wagner theorem [3], graphene previously was considered an unstable material because of its thermal fluctuations which would prevent the formation of materials with long range scale crystalline orders at specific/finite temperatures [4]. The exfoliation technique attracted more interest in research on carbon nanomaterials especially after 1991. At the same time, carbon nanotubes (CNTs) were introduced by Professor Sumio Iijima [5]. Now, graphene is considered an excellent source of material for electronics, sensor devices, and optics. Additionally, interest was ignited in its other unique properties such as its optical transparency, high carrier charges mobility, chemical stability, and low level of density [47].

These properties of graphene with outstanding configuration, specification, and multiple applications have encouraged researchers to investigate various methods for synthesizing graphene. In 2004, the first group to work on the "scotch tape" method for exfoliating graphene by considering Highly Ordered Pyrolytic Graphite (HOPG) was a Manchester group [2]. In this method, graphene is predefined as highly ordered pyrolytic graphite with a perfect crystal structure specification. The graphene is produced on a scale of micrometers.

Wet chemical exfoliation of graphene was performed via an ultrasonication treatment of graphite by using a variety of solvents such as polymer-organic [6] or organic solvents [7] with a surface energy matched to the type of desired graphene. This method produces graphene with smaller sizes. However, prolonged exposure to signification can cause damage to the graphene structure because graphene can be produced chemically from graphite. Graphene oxide (GO) could be derived by the Hummers [8], Brodie, or Staudenmaier [9] methods, which are followed by the sonication method and the resulting graphene oxide (GO) is dispersible in water.

This is expanded to the interaction between the oxygen functionalities and the water to the basal plane of graphene. Hence, the hydrophobicity of the graphene would be destroyed and transferred to hydrophilic function, which means the water would intercalate during mild sonication between the sheets of graphene [10]. Methods to reduce GO to graphene have been reported in various sources [11]. In addition to sonication, GO can be exfoliated thermally with high temperatures and inert conditions. Indeed, the oxygen will oxidize the carbon plane of GO to Co2 and form water in some parts. The expansion of gas between the graphene layers would be able to exfoliate the graphite [12].

The other volatile substance figures, such as ClF3 [13], are ignited to intercalate the graphene sheets. To separate the graphene sheets, thermal shock is useful to volatize them apart from each other [27]. Graphene has high electron mobility [22], a breaking strength level 200 times better than that of steel [23], a high level of thermal conductivity [24], and a high opacity that is capable of the required substrate in optical microscope standard [25] (see Figure 2) procedures. These properties, compared to those of others properties, demonstrate great potential in a variety of high-demand fields, including in electronics in cases when graphene is involved in the

construction of transistors or integrator circuits [26]. Exploration of graphene's properties in the production of ultra-capacitors with high conductivity is highly desirable [27].

Fig2: Graphene standard optical microscopy image (100 x resolutions)

2-2-Exfoliation of Graphene

The exfoliated graphene method is produced by mechanical exfoliation of a wafer of HOPG (see Figure 3). Highly ordered pyrolytic graphite is included in many vertically stacked layers of graphene. To achieve the required substrates, a special cutter was used to cut the SiO2 chip into smaller pieces and to transfer the exfoliated graphene on the top region. This method has been discussed in other research papers. In P. Blake et al., SiO2 with a thickness of 300 nm is used as a graphene substrate. Given this thickness, a single atom-layer of graphene should be visible under white light to the unequipped eye [25, 27]. The contrast between the substrate and the graphene flakes should be highly visible to the unequipped eye, particularly when a SiO2 on a Si substrate is considered due to the relative refraction of the Silicon, graphene,

and SiO2 substrate. Hence, Fresnel equations would predict the behavior of light at each transition point [25, 27]. The contrast can be used to identify graphene or graphite flakes in high-quality conditions. Flakes with more layers of carbon ignited with a darker color can be compared with graphene/graphite with fewer layers. As Blake's research paper shows, SiO2 with any thickness can be identified as long as the right filter is used. Five to six inches of scotch tape was discarded from the whole amount to prevent the tape from being polluted by dust in the air. Then, a new piece of scotch tapes was removed and pressed onto the shiny surface of the HOPG. The experiment needed to be repeated about ten seconds. After about ten seconds the tape was peeled away from the desired substrate and the shiny, thick layers of graphite remained stuck to the top substrate surface [27].

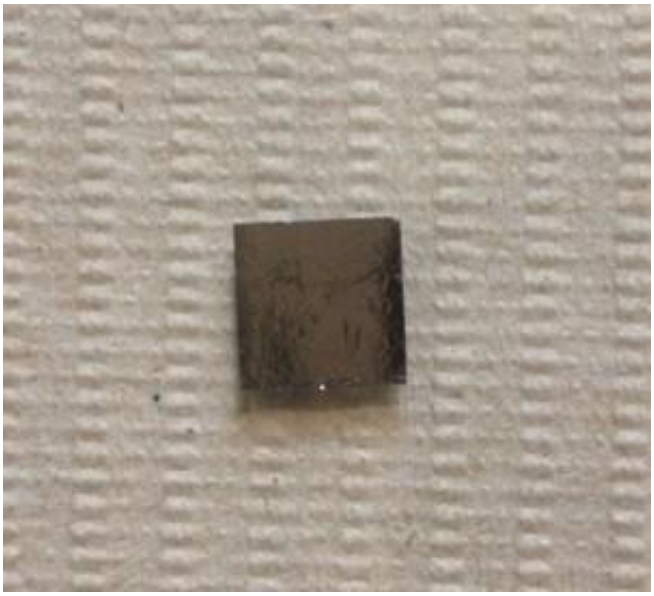

Fig3: HOPG wafer for making graphene flakes

2-3-Chemical Vapor Deposition Method

In the CVD method, chemical reaction has an important and effective role when compared to other types of film deposition techniques such as physical vapor deposition technique (PVD) [34]. The schematic of a CVD furnace is shown in Figure 4. The system includes removal of completed gas and reactor systems. As long as the chemical vapor deposition is in progress, the reactive gas will be fed by the gas and delivered to reactor which includes essential valves. Controllers manipulate the rates of passing and mixing units of gas in the system. Also, this section is responsible for mixing the variety of uniformed gases before reaching the reactor [34]. Furthermore, the heaters provided high temperatures. Eventually, a delivery system removes non-reacted gases from the system. Although the chemical vapor deposition is not an easy process to control, some additional parameters can be used to achieve the best results. Various parameters to consider during deposition techniques are pressure, temperature, and length of the reaction [34].

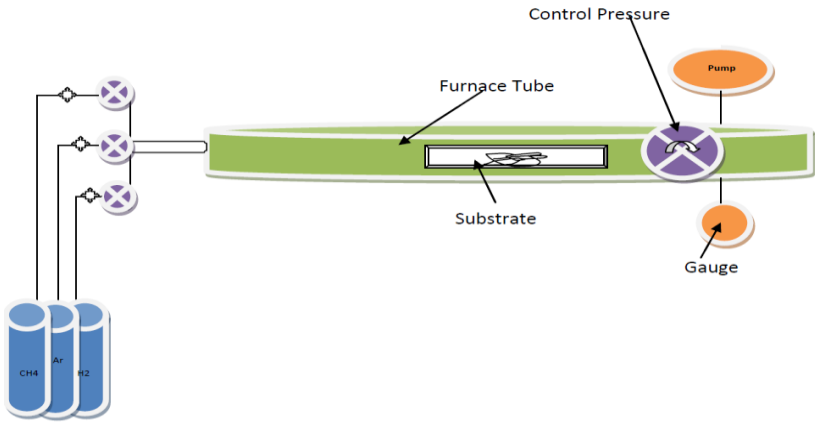

Fig 4: Schematic of a tube's furnace in a CVD system [34].

In a chemical vapor deposition process (see Figure 5), the kinetics of gas and chemical reactions are considered to be the most complicated parts in the convection system. According to fluid dynamics, the diffusion of reactive parts from the substrate or into the substrate is not an easy step to manage for each boundary layer. The formation of non-uniform thickness happens above the substrate. Hence, diffusion usually happens in the slower of two regions, such as in thick boundary layers, and sections of deposition may be non-uniform [34].

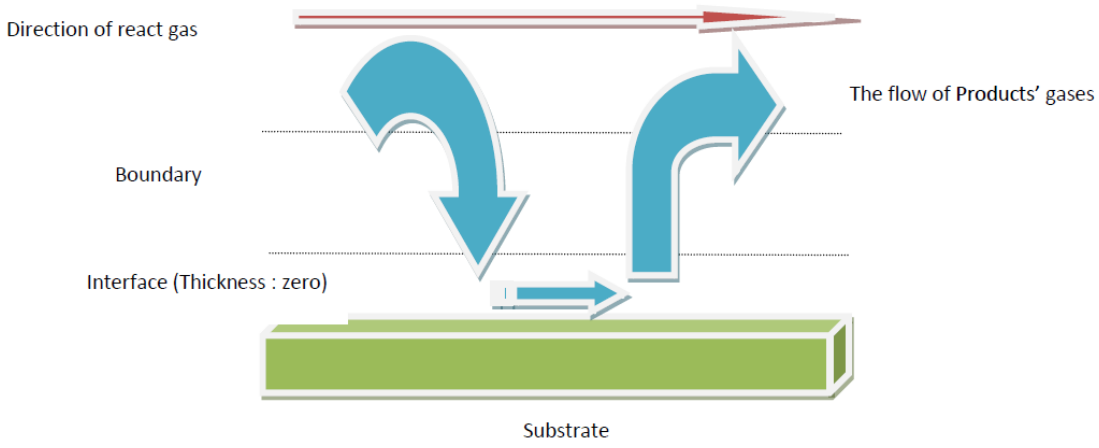

Fig 5: The process of chemical deposition in the CVD technique. First, the gas diffuses in boundary layers. Second, the reactant adsorbs above the surface substrate. Third, chemical reactions happen on top of the surface area. Fourth, the results of the reaction will desorbed by the surface, and diffusion will occur through the boundary layer [34].

2-4-Raman Spectroscopy

One of the best methods to determine the quantity of graphene layers in a sample is Raman spectroscopy. Raman scattering can identify the types of materials in each sample. All materials have a scattered light pattern that can be used to analyze wavelength shifts for various materials. Raman scattering can identify the types of materials in each sample. When light strikes the materials, two types of scattering are possible. The first is Rayleigh scattering and the second is Raman scattering. In Rayleigh scattering, the wavelength and photon of a given energy will interact with a molecule in the desired material and will raise its state with virtual energy [27].

After releasing another photon, the molecule returns to the original energy state. Accordingly, the molecule also returns to its original energy state after being raised. After the incident photon, the released photon remains in the same energy and wavelength. Moreover, Rayleigh scattering, as the energy of the photon is conserved and returned, is referred to as elastic process. Eventually, in Raman scattering, the photon's energy and relevant wavelength interact with a material's molecules in the same way as Rayleigh scattering to achieve a virtual energy level. However, when the molecule stops belonging to the virtual energy state, it does not drop back down to the relevant original state. Instead, there are more chances for it to drop and then to stay above or even below the original energy state. Hence, the molecule that drops to a lower state will release a photon; although, the energy level of that photon is not comparable with the incident photon. The released photon's energy depends on the final energy state of its molecule. If the original ground state is smaller than that of the final molecule's energy state, the released photon will have a lower energy state when compared to that of the incident photon. On the other hand, the longer wavelength, referred to as Stoke's Raman scattering, will considered as a premier incident [27].

The initial state is higher than the final energy state of the molecule; consequently, released photons will achieve a higher energy state than that of the incident photon. Then, anti-Stokes Raman scattering is used to detect the shorter wavelengths. Since the Raman scattering could be considered a formation of inelastic scattering, the energy of the photons is not maintained at an inelastic level. A visual representation of the concept of scattering levels and a comparison of differences between two elastic/inelastic properties is shown in Figure 6 [27].

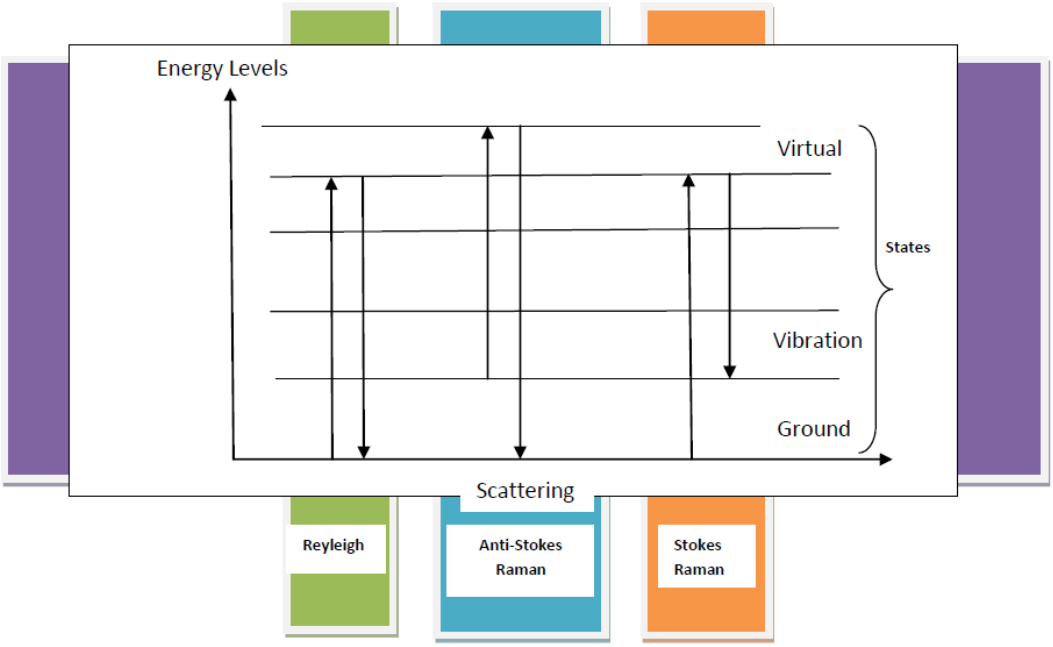

Fig 6: Different types of scattering [27]

For both Anti-Stokes and Stokes Raman scattering, energy removed from or transferred to the photon is connected to phonons and to the lattice vibrations of the material. Thus, there are some limitations to consider when changing photon energy state, frequency, and relevant wavelength.

The frequency shifts are different for each material. In scattered photons, shifts in the frequencies' measurements can shed light on the identity of the material type. Actually, the shift depends on the energy of the molecule's modes spacing. Also, the polarizability process is related to molecules' bond lengths and those with shorter bonds are harder to polarize [27].

In solids' crystalline aspects, modes are identified by the crystal structure to track the relevant polarization source and scattered light. The molecule will begin to vibrate if the polarizability of the molecule is starting to change which induces a dipole moment. Thus, unfixed conjunction polarizabilities produce Stokes and anti-Stokes scattering. As a result, all photons will be released by oscillating dipole moments. But Rayleigh scattering happens more frequently than either the other two types of Raman scattering (Stokes or anti-Stokes Raman scattering). Stokes Raman scattering occurs more often than anti-Stokes Raman scattering. But the photon energy shift will be the same either in Stokes and anti- Stokes Raman scattering shifts [27].

Due to its form and higher frequency of occurrence compared to anti-Stokes Ramen scattering and Stokes Raman scattering, Stokes scattering is used more in Raman spectroscopy measurements. Raman spectroscopy also has huge advantages compared to other types of spectroscopy, like infrared form. Hence, the non-destructive aspect does not need any sample preparation steps or a vacuum system. Thus, results can be produced more quickly and resolve maps of the various carbon forms within specific specimen [28], including in solid solutions, liquids, gases, and aqueous solutions [27].

Moreover, it can used in a wide range of temperatures, pressures [29], and with small samples [28]. (See Figure 7) Fiber optic cables have a great potential to be used in transmitting the readings necessary for remote testing procedures. Since the incident beams reflect without scattering, Raman spectroscopy is not as good of a candidate to analyze metals or alloys. Also, it is difficult to measure small concentrations of materials in a mixture because of Stokes scattering's low rate [27].

Raman spectroscopy is helpful to identify the number of layers present in a sample of graphene. Raman spectroscopy can provide a more recognizable frequency on multiple small layers of graphene and on other types of carbon allotropes like carbon nanotubes or CNTs. This is possible by comparing the positions and heights of the "so-called" D´ and G spectral lines, or peaks, from each sample which occurs near the 2700 cm^{-1} and 1580 cm^{-1} positions in the spectra [30, 31].

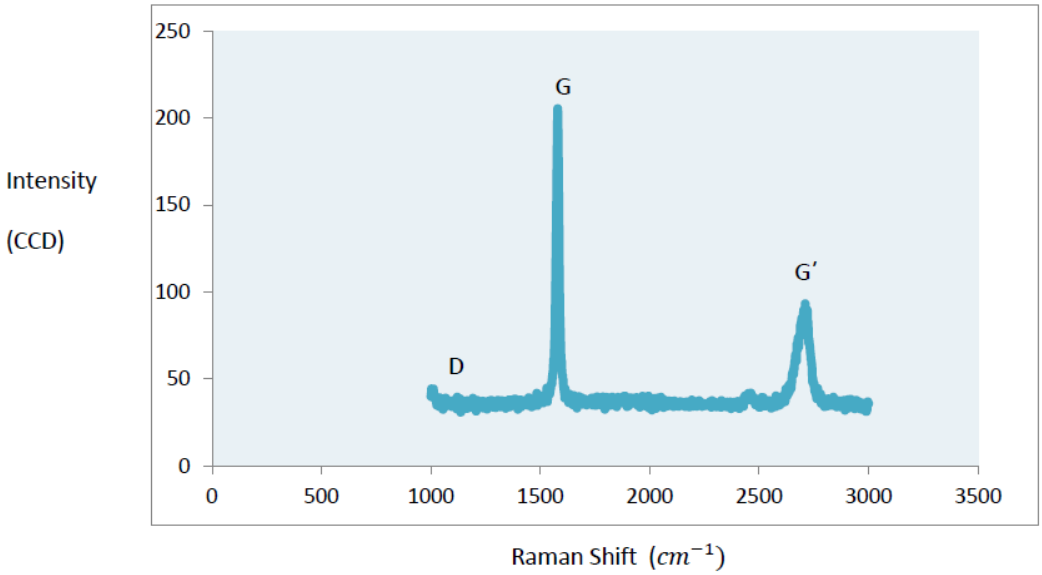

Fig7: Multi layers of graphene shown by Raman spectroscopy. (D= 1335) [27]

At G, the line indicates the quantity of graphene layers in the sample [27]. The single layer of graphene has just one single, sharp D′ peak; however, the higher orders are clearly composed of and distinguished by two different peaks. Also, more layers in the sample were shifted to the left side of the G shift. Indeed, more than five layers of graphene produce a related spectrum that resembles the HOPG forms [21]. It is important to keep in mind that Raman can only determine fewer than five or six layers in a sample to satisfy theory concepts [32, 27]. In the Raman spectra for monolayer graphene/graphite, the G band is shown at 1582 cm^{-1} and the G′ band appears in the region around 2700 cm^{-1} (see Figure 9) [30, 27]. Considering the edge region in this type of graphene sample, the result appeared as a "so-called" disorder induced in the DD-band and appeared as half of the frequency of the G′ band, which is around 1350cm^{-1}, using laser excitation of the graphene sample [31].

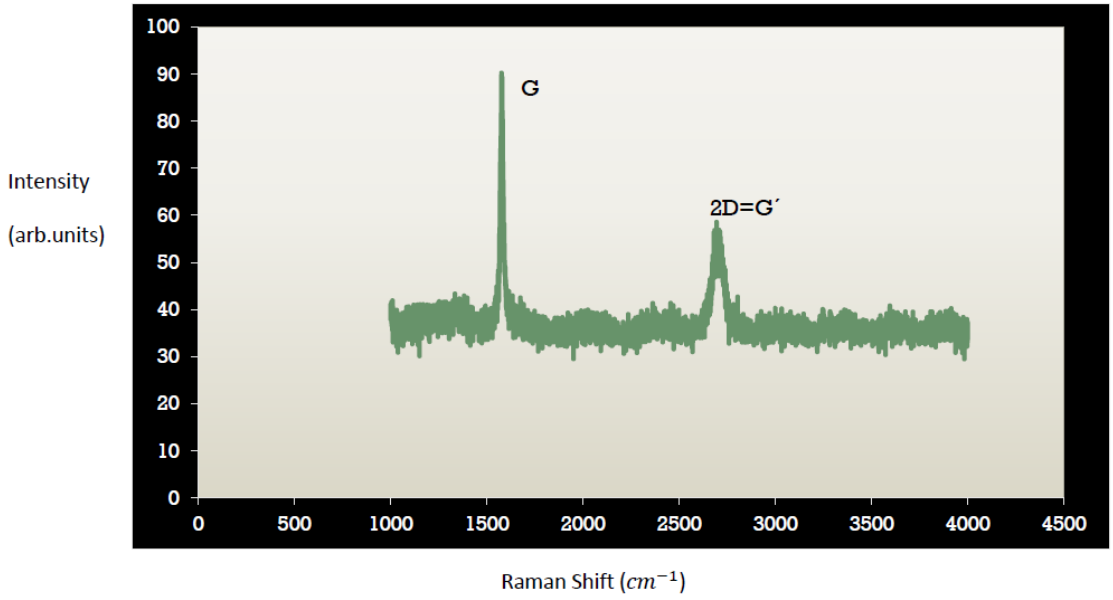

Fig 8: Graphene edge result using Raman spectrum [5]. The main features in Raman, the G and G′ bands are presented.

Clearly, the G band demonstrates double degenerates such as iTO and LO phonon mode. In fact, the G′ band is the only band coming from the first order of the normal Raman scattering process in the desired graphene sample. On the other hand, the G′ and D bands come from the second order process in graphene. Thus, the G′ band is involved in two iTO phonons near the area of the KK point and one iTO phonon can clearly be considered as a defect of the D band. Since the G′ band is almost twice the frequency of the D band, some publications have preferred to call it the 2D band (see Figures 8, 9) [27, 52].

Although two phonon bands are available in the second order of the Raman spectra, that does not indicate a defect or disorder in the graphene sample. To prevent any potential misleading connections with any disorder or defects, or confusion with two dimensional features, conventional notations such as "G′ G′ band" are usually used in scientific papers on graphene and nanotubes. Also, it useful for other types of notation, such as D′ D′ band, to signal other weak disorder aspects. In this paper, this feature appears in the ~1620 cm^{-1} section [52].

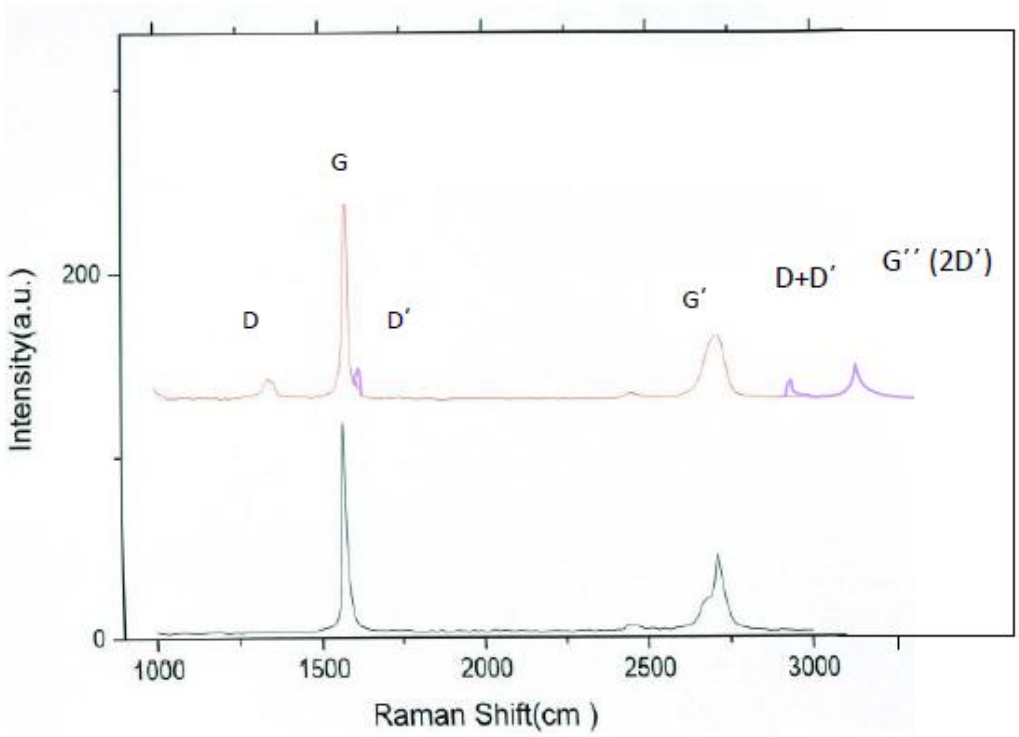

Fig 9: Graphene Raman shifts [53]

2-5-Atomic Force Microscopic

The atomic force microscopic has different parts, such as the cantilever and the probe, for scanning surfaces [16]. In the most cases, the cantilever is made by silicon and silicon nitride at the nanometer scale. When a tip is located in the desired surface region, the force between the tip and the sample causes cantilever deflection based on Hooke's law [16]. In this situation, various types of forces like capillary, Van Der Waals, and electrostatic are measured with atomic force microscopic instruments [37]. In addition to the various forces and the use of different types of probes, additional microscopy types such as scanning thermal microscopy, photo thermal microspectroscopy, and scanning joule expansion microscopy, are considered in the microscopic field. The other methods are optical interferometers, capacitive sensing, and piezoresistive cantilever atomic force microscopic [16].

The previously mentioned cantilevers are adjusted and provided with piezoresistive elements that act as strain gauges. Feedback reactions will adjust the tip to a certain and safe distance for a sample. Hence, the distance remains a secure constant force between the tip and the sample's surfaces [17, 18]. Generally in most AFMs, the tip or sample is placed on three piezo crystals that are responsible for scanning in three main directions (x, y, and z) [17] . In 1986, the atomic force microscopic was invented and new type of piezoelectric scanners and tube scanners were introduced to use in scanning tunneling microscope (STM) instruments for surface imaging at the atomic scale [18] . Later, tube scanners were added into AFMs. The tube scanner moves the sample by adjusting a single piezo tube with an interior contact and four different external contacts in the main three directions [17].

There are some advantages and disadvantages for using the tube scanner. The main advantages for the tube scanner include better condition for vibration isolation, a clearer result, and a clear frequency in the construction of a single crystal when the combination of isolation stage with low resonant frequency is more important [16]. But the disadvantage is that the x-y movement can cause unwanted z motion in the distortion step. Since the AFM is monitored in various modes and depending on the application process [17], the probe is counted as one the most important measurement devices in AFM instruments. The AFM probe has a sharp tip at the end of a free swinging area and a cantilever sticking out from a holder plate [19]. The cantilever's dimension is measured in micrometers and Atomic Force Microscopic probes are produced by MEMS technology [17].

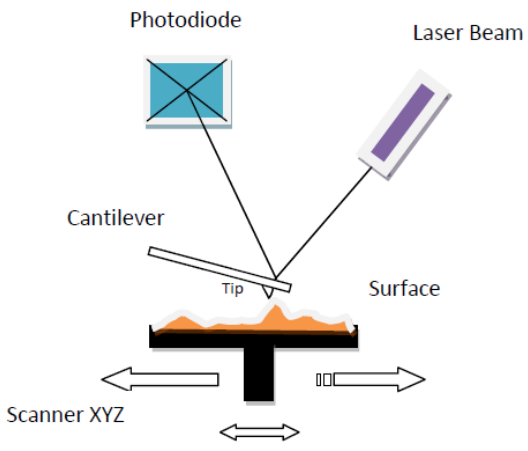

Fig 10: Schematic of beam detection in AFM [19, 16]

Clearly, atomic force microscopic has more advantages compared to those of a scanning electron microscope (SEM). A scanning electron microscope provides 2D images of a sample and an atomic force microscopic provides 3D/three-dimensional images [33]. Investigating the sample profile by AFM does not require any specific treatments, such as metal or carbon coatings, on the desired surface substrate. Also, AFM produces only a single scan image and scanning speed is limited. Hence, the limitations will not be limited to nonlinearity or piezoelectric creep [31] and the whole process must be monitored by special software [17, 38].

3-Proposed Research

3-1- CVD Growth of Graphene by Using Transitional/Catalyst Metals

Typically, the formation of graphene on transition metals by chemical vapor deposition happens based on a two-step mechanism. The first step is the dissolution or dilution of carbon into the metal source and the graphene is formed through a fast cooling process. This step is also known as the segregation process. Consequently, CVD is an easier method to obtain graphene with the desired growth features. Chemical vapor deposition is known to be produced by the decomposition of carbons, hydrocarbons or even polymers when heated metal sources are used as catalysts. For graphene growth purposes, various types of metals such as Ni, Pt, Cu, Ru, and Ir are used as catalysts. The number of graphene layers is monitored by the thickness and the type of catalyst. Also, the size of the graphene is related to catalyst size.

According to Blakely's group [39], the segregation of graphene on Ni surface involves heterogeneous composition in a thermal equilibrium process related to the relevant phase diagram region. In the precipitation region, the non-homogeneity corresponds to the equilibrium phase separation [40]. Further investigation by the authors showed that monolayer graphene with a specified segregation in the initial step is continued by graphite formation precipitation [41]. As Figure 11 indicates, the hydrocarbon molecules chemisorb on the metal surface (step 1) and dissociate in the dehydrogenation region (step 2). Then, the dissolute carbon adatoms will diffuse into the bulk metal surface (step 3). Clearly, the chemical absorption is ready to serve an electron associated with the empty d-shell of the transition metals.

As long as, the concentration of carbon adatoms in the bulk metal is in progress, the segregation process either will begin to achieve the nucleation threshold or reach the cooling step to decrease carbon solubility in the bulk metal. In the next step, the diluted carbon adatoms diffuse to the metal surface (step 4). Then, the segregation process for graphene formation is completed (step5). But it is necessary to keep in mind that the segregation process does not stop until the concentration of carbon in the bulk metal reaches the equilibrium stage [42].

The nucleation and equilibrium concentrations have different reactions in various operational conditions. The precipitation mechanism is applied to explain graphene formation for most types of transition metals [43].

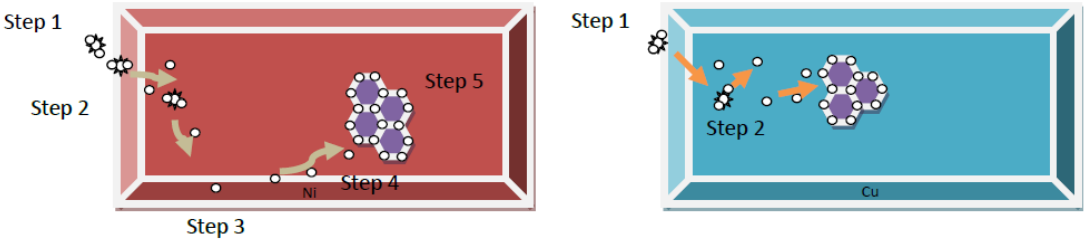

Bulk Growth

Surface Growth

Fig11: The formation of graphene on Ni and Cu [43].

Copper has a very low carbon solubility; consequently, the surface would need to be covered with a better deposition of the graphene growth mechanism. The growth would start after the hydrocarbon dissociation process and stop after the hydrocarbon supply source (see steps 1 and 2 in Figure 11). For example, temperature-programmed growth (TPG) is different from chemical vapor deposition. In the TPG method, the hydrocarbon is defused to the transition metal at room temperature. The empty d-shells in transition metals are the main source for hydrocarbon absorption. After heating up the hydrocarbon source, decomposition and nucleation of graphene growth happens at the appropriate temperature. The size of graphene produced with the TPG method is smaller than the graphene size produced by the CVD method. The different sizes of graphene growth depend on growth temperature conditions and the size ranges between nanometers and hundreds of nanometers [44]. Among all catalysts or metals considered for graphene formation, nickel and copper have the best potential to synthesize graphene growth even at large scales, but more research is needed to achieve controllable synthesis, better fabrication, size, and quantity of graphene's layers. These assumptions can be better understood if the graphene growth mechanism, growth kinetics, and limitation steps are clarified with a new generation of catalysts and growth processing procedures. Reusing catalysts and demonstrating effective separation skills to producing more graphene at lower costs and at reasonable production scales [15].

3-2- CVD Growth of Graphene on SiO2 Substrates Using Evaporated Metals

Using evaporated metals or a transfer-free technique is considered one of the main methods to synthesize graphene directly onto SiO2 substrates. Carbon is diffused through a layer of catalyst metals such as Ni, Cu, Co, Au, etc. As discussed above, Chemical Vapor Deposition is also a sufficient method to fabricate graphene with a controlled thickness on metal substrates [48]. For the next step, the achieved graphene films need to be removed from the metal substrates and transferred to enclosed substrates for further processing [49]. In the evaporated metal method, the bilayer graphene is formed directly on wrapping substrates, without employing any further transferring process. The solid carbon source is deposited between metal layers and wrapped onto the substrates. Finally, the bilayer of graphene is obtained at 1000°C [50].

For example, in the case of using nickel (Ni) as the evaporated metal source (see Figure 12), the carbon between the nickel and insulating substrates will penetrate into the nickel film. The graphene growth is formed on the top and bottom surfaces of the nickel metal after the cooling process. The formed graphene growth layers can appear as multi-layers and bilayers of graphene. To achieve the carbon source bilayer graphene on top of a nickel surface, carbon diffusion needs to form between the insulating or enclosing substrates and the nickel layers [47].

Carbon can be provided by various sources such as solid polymer films of poly methyl methacrylate (PMMA), acrylonitrile butadiene styrene (ABS), high impact polystyrene (HIPS), or a flow of methane gas on top of the nickel layers. The desired result is achieved by an annealing process under Ar and H2 gas flows at high temperatures of around 1000°C.

Thus, the carbon decomposes and diffuses into the evaporated metal layer (as in the Ni layer) and is placed on both sides of the nickel surface during the final formation, cooling, and annealing steps. The etchant region will be removed from the nickel surface and the bilayer graphene growth obtained directly on the SiO2 substrates [47].

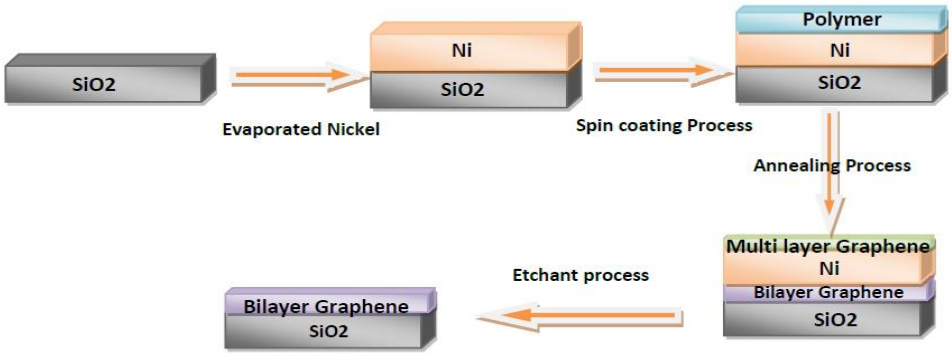

Fig12: Sketch of the graphene growth from carbon as a solid source [36]. Nickel film is thermally evaporated on top of a SiO2 substrate [47].

Copper can also be used as an evaporated metal source to receive graphene growth and graphene can be expanded over the surface by controlling the temperature range between 875 and 1000 °C. The method does not require the precipitation of metal on top of a polymer film. In addition, the graphene grains are associated and related to the copper grains. Consequently, graphene grain size could be increased by controlling the copper grain size [51].

3-3- CVD graphene growth by Exfoliated Graphene on SiO2 substrate

The mechanism growth of graphene on mechanically exfoliated graphene by chemical vapor deposition method is considered to be “surface adsorption” rather than bulk diffusion because of the short diffusion length [8]. To improve the quality of the graphene, various growth factors have been identified including the ratio of gas feeding, temperature growth, and pressure measurements [9, 10]. Additionally, the grain boundaries and exfoliated areas including corners, tops, and bottoms play an important role in nucleation seeds and the formation of large scale graphene growth on SiO2 substrate by the CVD method. To achieve graphene growth from exfoliated graphene seeds directly on SiO2 substrate by the CVD method, various transition metals are eliminated under different circumstances. Initial formation of graphene flakes may grow near exfoliated graphene grain boundaries, different magnifications surface areas, and tops and bottoms of intentionally exfoliated flakes.

4-Experiment

4-1-Cleaning the SiO2 Substrate

The SiO2 substrate is cut into 1-inch by 1-inch squares and each square of substrate is rinsed with acetone to dislodge and remove any large particles on the surface. The SiO2 substrate is then placed into a beaker containing acetone solution for 5 minutes. Acetone is used as the main cleaner to ensure the removal of any organic compounds or ionic salts that may be present on the SiO2 substrate prior to the exfoliated graphene and further growth processes. Then, the SiO2 is removed from the acetone container and rinsed with isopropyl alcohol to remove any residual particles of acetone that may remain. Acetone will remove the remaining compounds from the

surface. The substrate is then dried with a nitrogen gas flow. Nitrogen gas is the main source to dry the surface because it is a non-reactive gas. Moreover, the Nitrogen is able to eliminate any chance reactions due to the isopropyl alcohol.

The other approach to achieve a clean surface is to use Piranha solution. Piranha etches use hydrogen peroxide (H2O2) and sulfuric acid (H2SO4) to clean organic residues from the desired substrates. Since the mixture is a strong oxidizing source, it can also remove most organic textures. Piranha acid is a 3 to 1 mixture of sulfuric acid to a 30% hydrogen peroxide solution. Piranha etch is dangerous and should be used in safe conditions. Piranha solution is corrosive and a powerful oxidizer. To prepare the SiO2 substrate, the surface is cleaned by Acetone to remove all organic solvents. Then, the surface is washed with piranha solution [53, 55].

Piranha solution is produced by adding hydrogen peroxide to sulfuric acid and the mixture process should be done very slowly. The heat of the final solution could reach temperatures higher than 95°C. The hot and bubbling solution will clean organic compounds from substrates and hydroxylate surfaces [54, 55]. The cleaning process for SiO2 substrates takes 3 minutes. Then, the substrate is removed from the solution. For best results, the SiO2 substrate was cleaned for 1 minute and 15 seconds. After placing the cleaned substrates in Acetone for 5 more minutes, the SiO2 substrates were dried with a nitrogen gas flow. Once the substrate is dried, it is ready for the placement of the exfoliated graphene on its top surface. All substrates were investigated by optical microscopic to choose those with the best conditions. In some disposal cases, the Piranha acid caused too many corrosive defects on the top of the SiO2 substrates [55].

4-2- Exfoliated Graphene

After cleaning the SiO2 substrate, the layers of graphene from the HOPG wafer were exfoliated onto the surface. First, the layers of HOPG were peeled away by 3M sticky tape. Then, two layers of tape were pressed together several times until the graphite sheets remained on the sticky side of the tape. The final result was large portions of non-shiny graphite layer/layers. The ideal situation is to achieve a region with less glue residue than on the SiO2substrate. Although, the tape residue does not have a serious effect on the quality of the graphene flakes, it would make it hard to find the desired flake regions on the SiO2 substrate [27]. Then, the shiny side of the SiO2 substrate was placed on the regions with flakes with a tweezer and pressed into place for several seconds. The substrate was removed from the sticky tape and the sample was ready for the next step. This process was repeated for each SiO2 substrate. Additionally, the dull graphite region could be used for producing various substrates (see Figure 13) [27].

Fig 13: Exfoliated graphene technique. “Scotch” tape is pressed to the HOPG and folded several times.

The SiO2 sample was placed underneath the optical microscope to identify graphite flakes. The transferred flakes were captured by a built-in color camera in the Raman spectroscopic instrument (see Figure 14). Various regions were investigated to find one layer or multi layers of graphite flakes. Different flakes and layers appeared in different colors during the observation process. The multi layers flakes indicated that few carbon layers were present in that specific region. On the other hand, the Raman spectroscopic results revealed a number of carbon sheet layers [27].

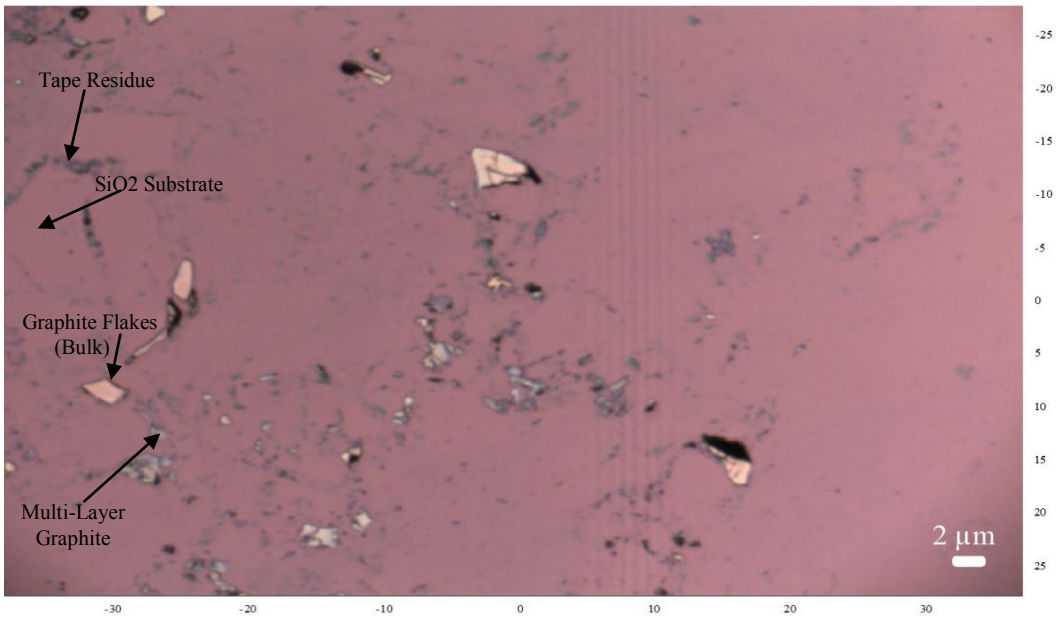

Fig14: Graphite flakes result using optical microscope (10 x resolutions)

The desired flake was analyzed (see Figure 10) to investigate the desired region. Then, the spectrometer was closed, the light turned off, and the barrier opened so that the sample was struck by a laser beam [17]. The process readings were sorted by computer program. All surface data were combined to produce Raman shifts. The final spectrum, structural information of desired peaks, and data were characterized by Lorentz distributions analysis. Finally, the result identified the number of graphene layers in each flake sample [27].

4-3- CVD Growth Conditions

Chemical vapor deposition occurs in low pressure conditions in a tube furnace system. The SiO2 substrate and exfoliated graphene flakes on the top region were placed into the furnace. The tube was sealed at both ends by two stainless end caps. Then, the sample was placed directly in the center of the furnace to avoid heat loss at each side of the furnace. Once the tube is sealed, the furnace is evacuated by a rotary pump. A pressure of 5 torr was chosen to remove air during the growth process. To achieve the best results, different recipes to synthesize graphene were examined. Below are some selected recipes used to synthesize graphene (see Figure 15):

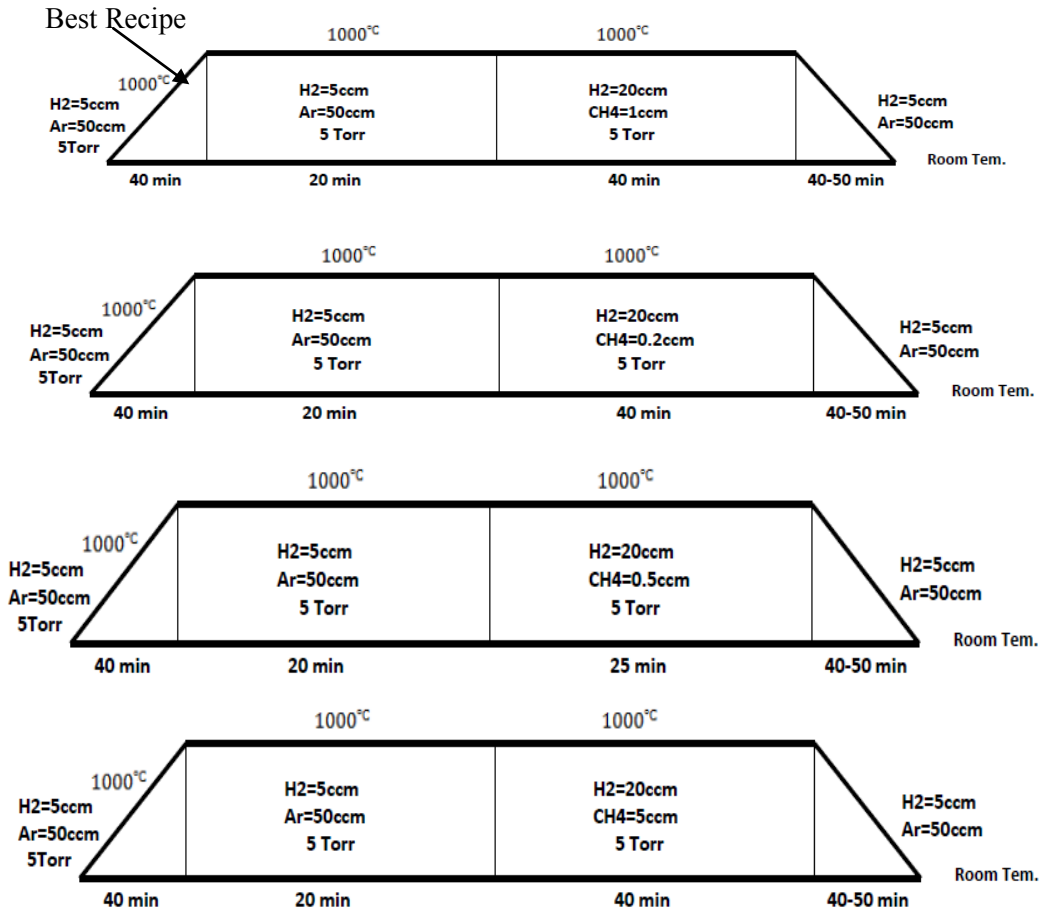

Fig15: Different recipes used to synthesize graphene in a CVD furnace

Figure 15 shows illustrations of the four recipes which were used during the experiment process. The difference in the last three recipes is concentrated in the amount of time used for graphene growth and methane gas flow. In the first recipe, an increase in growth speed and deposition was observed by changing the methane fellow to 1scc. Then, graphene growth occurred on top of the exfoliated regions. In other words, increasing methane fellow provided better conditions for graphene growth on top of exfoliated flakes.

4-4- Results and Discussion

Figure 16 presents optical images of exfoliated graphene flakes on SiO2 substrate before Chemical Vapor Deposition. After choosing the regions to observe in detail, such as those shown in Figure 17, the different types of graphene layers on a SiO2 substrate was indicated by mechanically exfoliated graphene. Different regions were used to check different layers of graphene as well as relevant thickness and roughness by Raman spectroscopy and Atomic Force Microscopy.

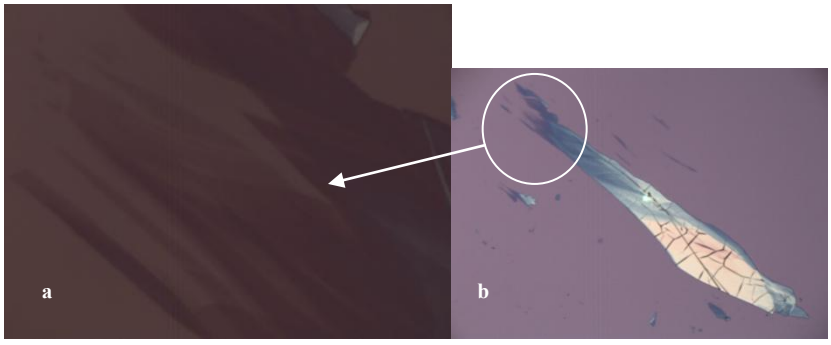

Fig16: Optical images of exfoliated graphene regions before CVD. (a) Indicates the considered whole flake of exfoliated graphene with a magnification of 10x, (b) shows the same area at 100x optical resolution for characterizing purposes.

Then, the laser Raman targets different areas of the exfoliated graphene flakes by considering different color shades of graphene and thickness. The result is provided by Raman spectroscopy (see Figures 17-19).

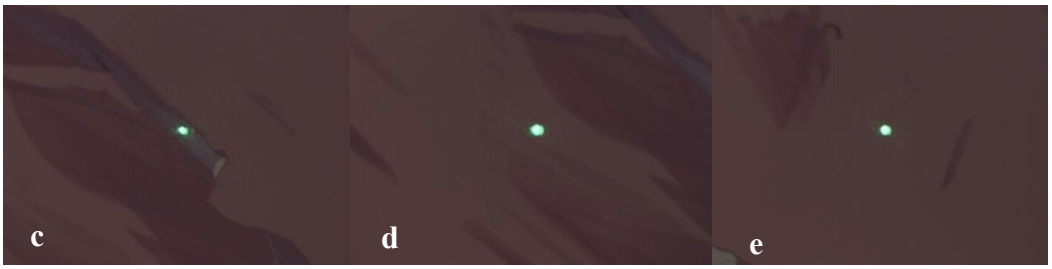

Fig 17: Laser points on various regions to achieve Raman shifts before CVD growth.
(c, d, e) Optical Images of bulk, multilayer, and bilayer graphene samples obtained of exfoliated graphene on SiO2 substrate before CVD at a magnification of 100x.

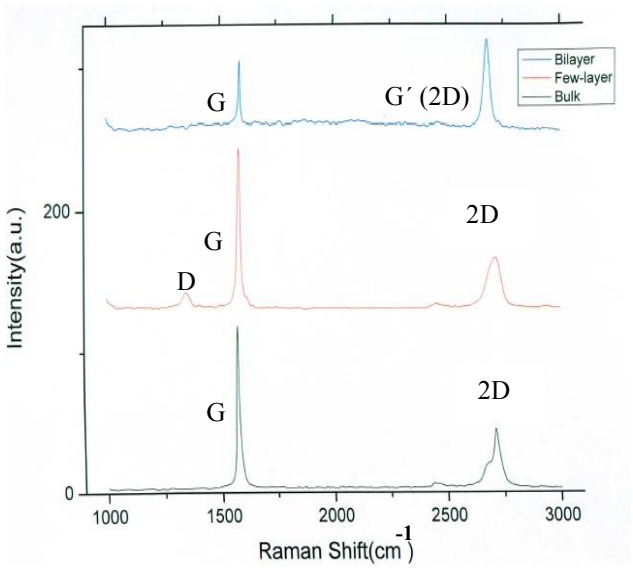

Fig 18: Raman spectroscopy of graphene synthesis before Chemical Vapor Deposition growth

Three captured Raman peaks were of particular interest: the D peak at around 1360cm^{-1}, the G peak at ~1580 cm^{-1} and the 2D peak at ~2670cm^{-1}. The D peak originates from defects within the graphene layer. The G peak's intensity is due to the number of graphene layers in the sample. The 2D peak is the overtone of the D peak and is present even in the absence of any defects. The location and shape of the 2D peak are sensitive to the thickness of the graphene. Then, these regions were examined by atomic force microscopic before the CVD. The results of the collected regions are shown in Figure 19 (a, b, c):

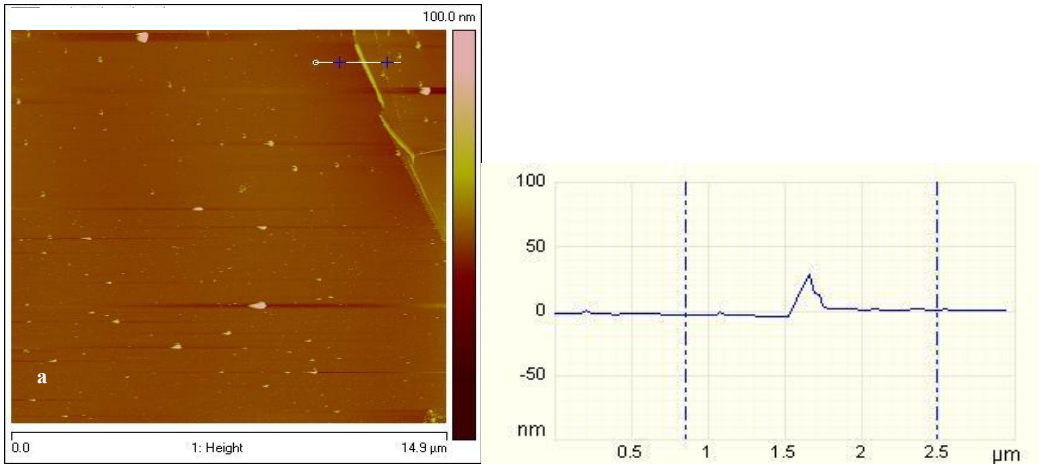

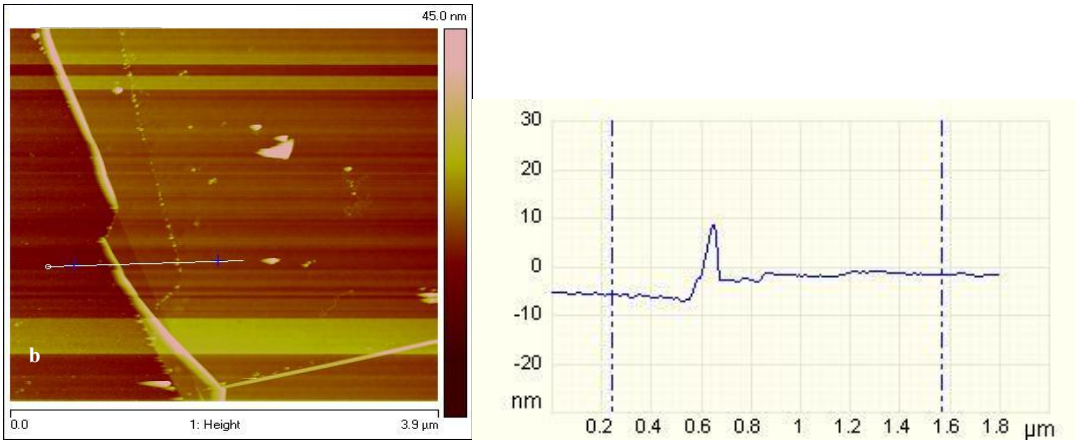

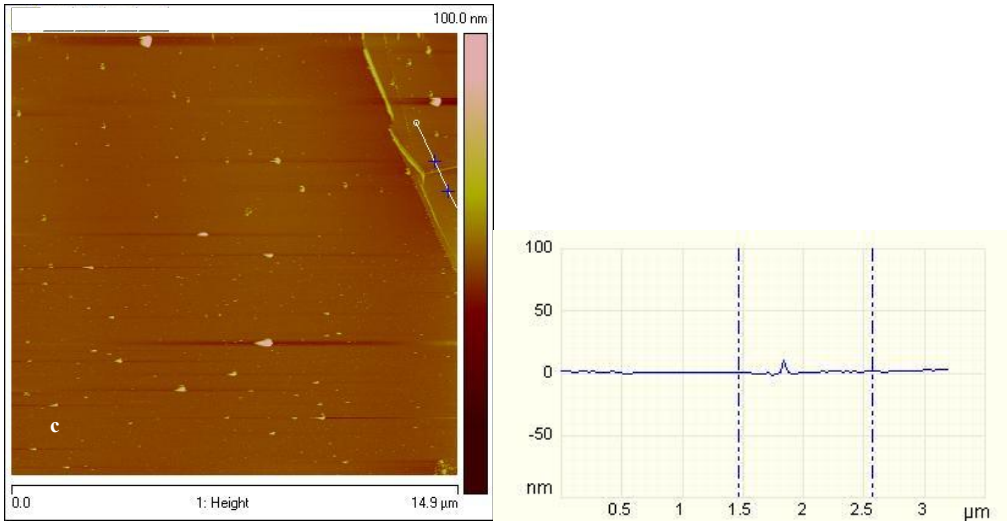

Fig 19: (3) AFM images of the exfoliated graphene before CVD growth. (a)The surface and the substrate at the edge region, and (b, c) height in different areas.

In order to confirm the possibilities of graphene on exfoliated graphene regions during the CVD growth, the desired sample was placed in the furnace tube. The furnace was evacuated to a base pressure of 5 torr at room temperature (23 °C) (see Figure 22). Air was removed during the process and then 50 sccm of Ar was introduced into the chamber for 40 minutes to replace the air before heating the furnace to the annealing/growth temperature of 1000 °C. During all heating stages, the flow rate of H2 gas was 5 sccm. After annealing with the same H2 flow rate for 20 minutes, CH4 was introduced to the furnace at a flow rate of 1 sccm during the growth stage for 40 minutes.

Fig 20: Original images of chemical vapor deposition furnace

After the growth time of 40 min, the flow of CH4 was shut off, and the furnace was allowed to cool down naturally with a hydrogen flow of 5sccm and Ar of 50sccm for 40-50 min. The sample was removed from the furnace at room temperature and the regions of interest were examined with the optical microscope (see Figures 21, 22).

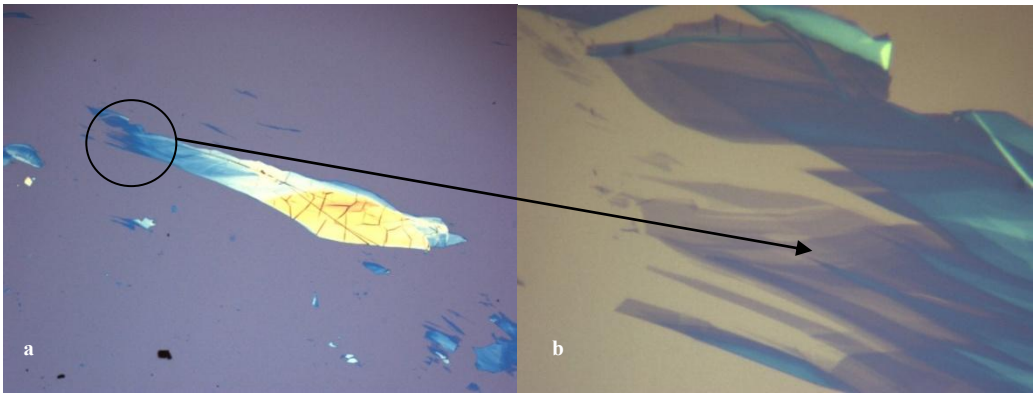

Fig 21: Optical images of exfoliated graphene layers/regions after CVD. (a) Indicates the considered whole flake of exfoliated graphene with a resolution of 10x, (b) shows the same area at 100x optical resolution for characterizing purposes.

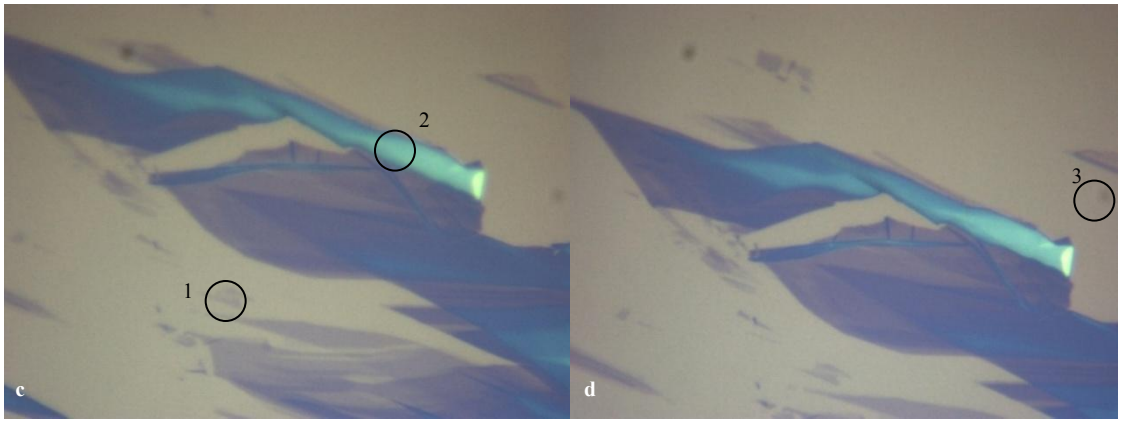

Fig 22: Selected same regions to achieve Raman shifts changes after CVD growth. The same regions were selected to show the Raman shift changes after the chemical vapor deposition process .(1,2,3) Indicate the bulk, multilayer, and monolayer/bilayer of exfoliated graphene on a SiO2 substrate after CVD at 100x resolution using an optical microscope

To elucidate the morphological dependence more clearly, the CVD graphene growth on top of the mechanically exfoliated graphene areas was further investigated. After chemical vapor deposition increased, layers of graphene and defects increased on top of exfoliated flakes. For this reason, AFM figures are shown to identify the differences (see Figures 19, 24, 25). Also, the different shades of color in images captured by optical microscopic are another reason to demonstrate the graphene growth mechanism (see Figure 16b, 21a).

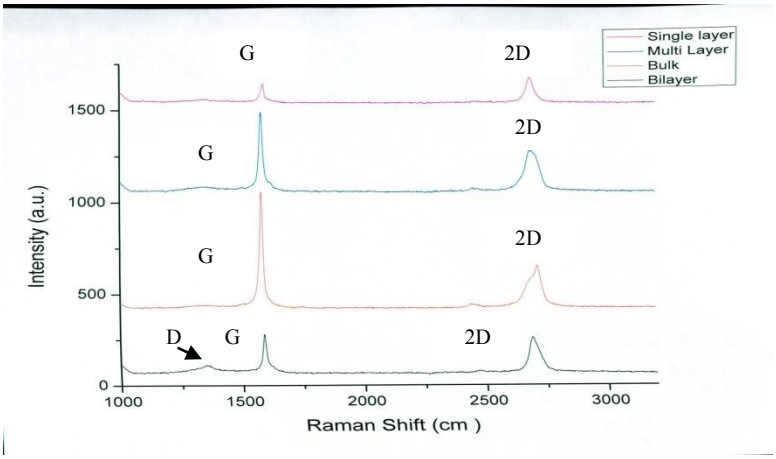

Fig 23: Raman spectroscopy of graphene synthesis after CVD growth

In Figure 23, the Raman spectrum characteristic depends on the thickness of the graphite film identification and identifies the comparison of different layers of graphene after growth. Based on transforming on top on exfoliated flakes, increased layers are observed. The multilayer transfer to bulk, bilayer, and monolayer after CVD growth changed to multilayer. New monolayer and bilayer graphene growths also appeared.

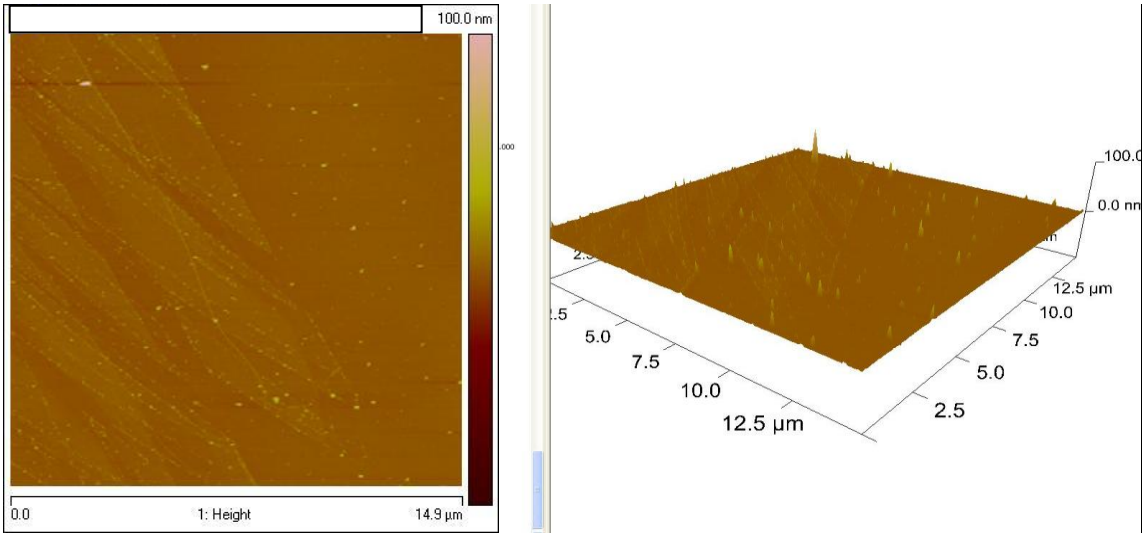

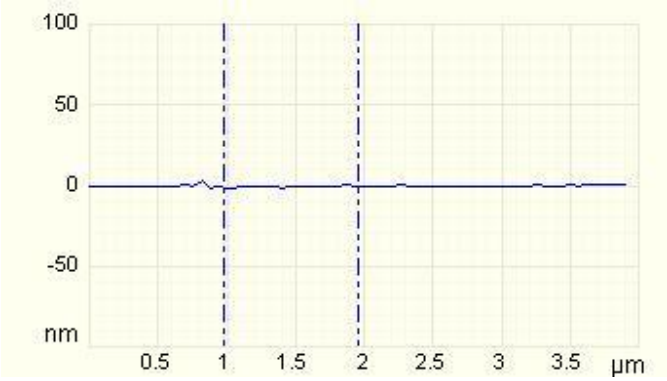

Fig 24: AFM images of the exfoliated graphene after CVD growth on edge. The graphene growth in some regions happened on the top surface as well as on the vertical and horizontal.

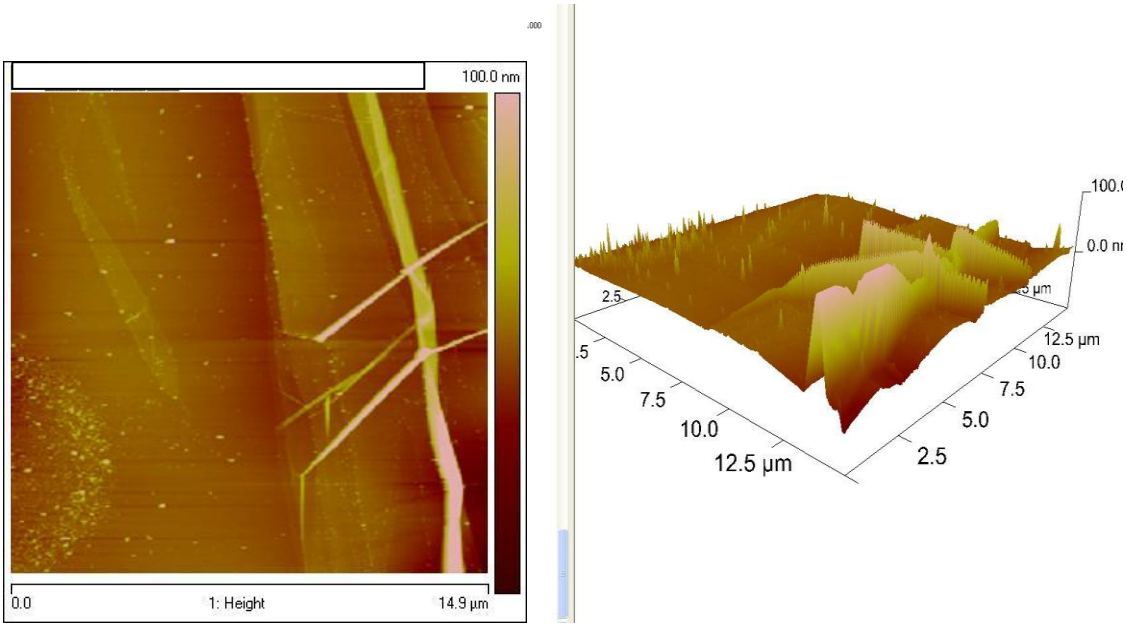

Fig 25: AFM images of the exfoliated graphene after CVD growth in bulk region. The surface has become more damaged with different heights in different areas.

The Atomic Force Microscope (AFM) image in Figure 25 demonstrates the growth of graphene layers on top of the exfoliated graphene surface. After CVD growth, there is evidence of increasing density, roughness, and height on top of the exfoliated flakes. Before CVD growth, all received data such as Raman spectroscopy and AFM indicated various types of exfoliated regions (see Figures 18, 19). Hence, specific regions were investigated to clarify the relevant layers as well as the roughness and the thickness of the flakes. The same regions were again investigated after CVD growth (see Figures 23, 24, 25). There was clear evidence of increasing roughness and stacking growth on top of the exfoliated graphene. A comparison of figures 18 and 23 shows the increase of graphene layers by Raman spectroscopy. The same regions were investigated throughout the process. Furthermore, all these regions were collected by AFM to compare surface roughness and growth process before and after chemical vapor deposition. For this reason, the multilayer flakes in edge areas were selected and a 3D AFM demonstrated an increased roughness and vertically stacked layers on top of the flakes after the CVD process.

5- Conclusion

Graphene is a novel material that possesses various desirable properties, and CVD appears to be the most promising route for accomplishing graphene synthesis and growth in a scalable way. However, the mechanical exfoliation of HOPG is not suitable for mass-producing large-area graphene sheets, but is considered as the defect surface to produce more graphene sheets through the Chemical Vapor Deposition growth process. The formation of graphene on exfoliated graphene through CVD followed a two-step process. The first step was the dilution or incorporation of carbon on the exfoliated graphene regions followed by the formation of graphene through rapid cooling, also known as segregation, to achieve graphene growth. These results show that graphene growth is achieved both before and after CVD as indicated by Raman peaks, optical images, and AFM differences. As a result, graphene growth appeared on top of exfoliated flakes as vertical stacking layers after CVD growth.

6- References

1- A. Bianco, H.-M. Cheng, T. Enoki, Y. Gogotsi, R.H. Hurt, N. Koratkar , "All in the Graphene Family: A Recommended Nomenclature for Two-Dimensional Carbon Materials," *Carbon* , vol. 65, pp. 1-6, 2013

2- K.S. Novoselov, A.K. Geim, S.V. Morozov, D. Jiang, Y. Zhang, S.V. Dubonos, " Electric Field Effect in Atomically Thin Carbon Films, " *Science*, vol. 306, pp. 666-669, 2004

3- N.D. Mermin, H. Wagner, "Absence of Ferromagnetism or Antiferromagnetism in One- or Two-Dimensional Isotropic Heisenberg Models," *Phys Rev Lett*., vol. 17, no. 22, pp. 1133‑1136, 1966

4- N.D. Mermin, "Crystalline Order in Two Dimensions," *Phys Rev.*, vol. 176, no. 1, pp. 250-254, 1968

5- S. Ijima, "Helical Microtubules of Graphitic Carbon," *Nature*, vol. 354, pp. 56-58, 1991

6- Y.T. Liang, M.C. Hersam, "Highly Concentrated Graphene Solutions via Polymer Enhanced Solvent Exfoliation and Iterative Solvent Exchange," *J Am Chem Soc.*, pp. 17661-17663, 2010

7- Y. Zhu, S. Murali, W. Cai, X. Li, J.W. Suk, J.R. Potts, "Graphene and Graphene Oxide: Synthesis, Properties, and Applications," *Adv Mater*, vol. 22, no. 35, pp. 3906-3924, 2010

8- W.S. Hummers, R.E. Offeman, "Preparation of Graphitic Oxide," *J Am Chem Soc.*, vol. 80 no. 6, pp. 1339, 1958

9- L. Staudenmaier, "Method for Representing The Graphite Acid," *Reports of the German Chemical Society*, vol. 31, no. 2, pp. 1481-1487, 1898

10- M.J. Allen, V.C. Tung, R.B. Kaner, "Honeycomb Carbon: A Review of Graphene," *Chem Rev.*, vol. 110, no. 1, pp. 132-145, 2009

11- S. Pei, H.-M. Cheng, "The Reduction of Graphene Oxide," *Carbon*, vol. 50, no. 9, pp. 3210-3228, 2012

12- M.J. McAllister, J.-L. Li, D.H. Adamson, H.C. Schniepp, A.A. Abdala, J. Liu, "Single Sheet Functionalized Graphene by Oxidation and Thermal Expansion of Graphite, *Chem Mater*, vol. 19, no. 18, pp. 4396-4404, 2007

13- J.H. Lee, D.W. Shin, V.G. Makotchenko, A.S. Nazarov, V.E. Fedorov, Y.H. Kim, "One-Step Exfoliation Synthesis of Easily Soluble Graphite and Transparent Conducting Graphene Sheets," *Adv Mater*, vol. 21, no. 43, pp. 4383-4387, 2009

14- J. Robinson, X. Weng, K. Trumbull, R. Cavalero, M. Wetherington, E. Frantz, "Nucleation of Epitaxial Graphene on SiC (0 0 0 1)," *ACS Nano*, vol. 4, no. 1, pp. 153-158, 2009

15- C.M. Seah, S.P. Chai, A.R. Mohamed, "Mechanisms of Graphene Growth by Chemical Vapour Deposition on Transition Metals," *Carbon*, Vol. 70, pp. 1-21, 2014

16- B. Cappella, G. Dietler, "Force-Distance Curves by Atomic Force Microscopy," *Surface Science Reports*, vol. 34, pp. 1-104, 1999

17- G. Binnig, C.F. Quate, "Atomic Force Microscope, "*Physical Review Letters*, pp. 930-933, 1986

18- G. Binnig, D.P.E. Smith, "Single-Tube Three-Dimensional Scanner for Scanning Tunneling Microscopy," *Review of Scientific Instruments*, vol. 57, No. 8, pp. 1688, 1986

19- P.J. Bryant, R.G. Miller, R. Yang, "Scanning Tunneling and Atomic Force Microscopy Combined," *Applied Physics Letters*, pp. 2233-2235, 1988

20- K. S. Novoselov, D. Jiang, F. Schedin, T. J. Booth, V.V. Khotkevich, S.V. Morozov, A. K. Geim, "Two-Dimensional Atomic Crystals," *Proc. Natl. Acad. Sci. U.S.A.*, vol. 12, pp. 10451-10453, 2005

21- A. Ferrari, "Exploring Graphene," *Solid State Communication*, vol. 143, pp. 47-57, 2007

22- A.K. Geim, K.S. Novoselov, "The Rise of Graphene," *Nature Materials*, pp.183-191, 2007

23- A. B. Kuzmenko, E.van Heumen, F. Carbone, D. van der Marel, "Universal Optical Conductance of Graphite," *Phys Rev Lett*., vol. 100, 2008

24- A.A. Balandin, S.Ghosh, W.Bao, I.Calizo, D.Teweldebrhan, F. Miao, C.N. Lau, "Superior Thermal Conductivity of Single-Layer Graphene," *Nano Letters*, pp. 902-907, 2008

25- P. Blake, K. S. Novoselov, A. H. Castro Neto, D. Jiang, R. Yang, T. J. Booth, A. K. Geim, E. W. Hill, "Making Graphene Visible," *Appl. Phys. Lett.*, vol. 91, 2007

26- M.D. Stoller, S. Park, Y. Zhu, J. An, R.S. Ruoff, "Graphene-Based Ultracapacitors," *Nano Lett.*, vol. 8, pp. 3498-3502, 2008

27- C. Reeves, Graphene:Characterization after Mechanical Exfoliation, *Senior Research*, College of William & Mary, Williamsburg, Dept. Physics, 2010

28- S. Prawer, R.J. Nemanich, "Raman Spectroscopy of Diamond and Doped Diamond," *Philosophical Transactions of the Royal Society of London. Series A, Mathematical, Physical and Engineering Sciences*, vol. 362, pp.2537-2565, 2004

29- Q. Zhao, H.D. Wagner, "Raman Spectroscopy of Carbon–Nanotube–Based Composites," *Phil. Trans. R. Soc. Lond. A*, vol. 362, pp. 2407-2424, 2004

30- A. C. Ferrari, J. C. Meyer, V. Scardaci, C. Casiraghi, M. Lazzeri, F. Mauri, S. Piscanec, D. Jiang, K. S. Novoselov, S. Roth, A. K. Geim, "Raman Spectrum of Graphene and Graphene Layers," *Phys. Rev. Lett*., vol. 97, 2006

31- D. Graf , F. Molitor , K. Ensslin , C. Stampfer , A. Jungen , C. Hierold , L. Wirtz, " Spatially Resolved Raman Spectroscopy of Single-and Few-Layer Graphene," *Nano Lett.,* vol. 7, no. 2, pp. 238-242, 2007

32- S. Reich, C. Thomsen, "Raman Spectroscopy of Graphite," *Phil. Trans. R. Soc. Lond. A*., vol. 362, pp. 2271-2288, 2004

33- X. Xu, A. Raman, "Comparative Dynamics of Magnetically, Acoustically, and Brownian Motion Driven Micro Cantilevers in Liquids," *J. Appl. Phys.*, vol.102, 2007

34- C. Miao, C. Zheng, O.Liang, Y.H. Xie, "Chemical Vapour Deposition of Graphene," *Phys Apps*., pp. 37-57, 2011

35- A. Kumar ,C. H. Lee, "Synthesis and Biomedical Applications of Graphene: Present and Future Trends," *Advances in Graphene Science,* pp. 5772-5578, 2013

36- K. J. Seu, A. P. Pandey, F. Haque, E. A. Proctor, A. E. Ribbe, J. S. Hovis, "Effect of Surface Treatment on Diffusion and Domain Formation in Supported Lipid Bilayers" *Biophysical Journal*, pp. 2445-2450, 2007

37- N.A. Geisse, "AFM and Combined Optical Techniques," *Materials Today*, vol. 12, pp. 40-45, 2009

38- R.V. Lapshin, "Analytical Model for The Approximation of Hysteresis Loop and Its Application to the Scanning Tunneling Microscope," *Review of Scientific Instruments*, pp. 4718-4730, 1995

39- J.C. Shelton, H.R. Patil, J.M. Blakely, "Equilibrium Segregation of Carbon to A Nickel (1 1 1) Surface: A Surface Phase Transition," *Surf Sci.*, pp. 493-520, 1974

40- X. Li, W. Cai, L. Colombo, R.S. Ruoff, "Evolution of Graphene Growth on Ni and Cu by Carbon Isotope Labeling," *Nano Lett.*, pp. 4268-4272, 2009

41- M. Eizenberg, J.M. Blakely, "Carbon Monolayer Phase Condensation on Ni(1 1 1)," *Surf Sci.*, pp. 228-236, 1979

42- E. Loginova, N.C. Bartelt, P.J. Feibelmarr, K.F. McCarty, "Factors Influencing Graphene Growth on Metal Surfaces," *New J Phys*., vol. 11, 2009

43- M. Losurdo, M.M. Giangregorio, P. Capezzuto, G. Bruno, "Graphene CVD Growth on Copper and Nickel: Role of Hydrogen in Kinetics and Structure," *Phys Chem Chem Phys*., pp. 20836-20843, 2011

44- M. Kralj, I. Pletikosić, M. Petrović, P. Pervan, M. Milun, A.T. N' Diaye, "Graphene on Ir(1 1 1) Characterized by Angle-Resolved Photoemission," *Phys Rev B - Condens Matter Mater Phys*., 2011

45- T.F. Chung, T.Shen, H.Cao, L.A. Jauregui, W. Wu, Q. Yu, D. Newell, Y.P. Chen , "Synthetic Graphene Grown by Chemical Vapor Deposition on Copper Foils," *Int. J. Mod. Phys.*, 2013

46- K.S. Novoselov, A.K. Geim, S.V. Morozov, D. Jiang, Y. Zhang, S.V. Dubonos, I.V. Grigorieva, A.A. Firsov, "Electric Field Effect in Atomically Thin Carbon Films," *Science*, pp. 666-669, 2004

47- Z. Peng, Z. Yan, Z. Sun, J.M. Tour, "Direct Growth of Bilayer Graphene on SiO2 Substrates by Carbon Diffusion through Nickel," *ACS Nano*., vol. 5, pp. 8241-8247, 2011

48- Y. Zhang, T. Tang, C. Girit, Z. Hao, M.C. Martin, A. Zettl, M.F Crommie, Y.R. Shen, F. Wang, "Direct Observation of a Widely Tunable Band Gap in Bilayer Graphene," *Nature*, pp. 820-823, 2009

49- A. Reina, X., J. Ho, D. Nezich, H. Son, V. Bulovic, M.S. Dresselhaus, J. Kong, "Large Area, Few-Layer Graphene Films on Arbitrary Substrates by Chemical Vapor Deposition, "*Nano Lett*., pp. 30-35, 2009

50- Z. Yan, Z. Peng, Z. Sun, J.Yao, Z. Liu, P.M. Ajayan, J.M. Tour, "Growth of Bilayer Graphene on Insulating Substrates," *ACS Nano*., 2011

51- L. Tao, J. Lee, H. Chou, M. Holt, R.S. Ruoff, D. Akinwande, "Synthesis of High Quality Monolayer Graphene at Reduced Temperature on Hydrogen-Enriched Evaporated Copper (111) Films," *ACS Nano*, pp. 2319-2325, 2012

52- F. Tuinstra, J.L. Koeing, "Raman Spectrum of Graphite," *phys.chem*., vol. 53, 1970

53- L.M. Malard, M.A. Pimenta, G. Dresselhaus, M.S. Dresselhaus, "Raman spectroscopy in graphene," *Physics Reports*, pp. 51-87, 2009

54- *Piranha*, Pennsylvania Univ., Laboratory Safety Manual, 2011

55- B. Hamilton, "Section-16.Laboratory Procedures," *Sci.chem.FAQ*, Part 4 of 7, 2008

56- S. Zhao, S.P. Surwade, Z. Li, H. Liu, "Photochemical Oxidation of CVD-Grown Single Layer Graphene, *Nanotechnology*, vol. 23, 2012

57- J. Kedzierski, P.L. Hsu, P. Healey, P.W. Wyatt, C.L. Keast, M. Sprinkle, C. Berger, W.A de Heer, "Epitaxial Graphene Transistors on SiC Substrates," *IEEE Transactions on Electron Devices*, vol. 55, pp. 2078-2085, 2008